A Spatial Analysis of Physiological Changes Associated with Infection of Cotyledons of Marrow Plants with Cucumber Mosaic Virus[1]

László I. Técsi, Alison M. Smith, Andrew J. Maule, and Richard C. Leegood*

Robert Hill Institute and Department of Animal and Plant Sciences, University of Sheffield, Sheffield, United Kingdom, S10 2TN (L.I.T., R.C.L.); and John Innes Centre for Plant Science Research, Colney Lane, Norwich, United Kingdom, NR4 7UH (A.M.S., A.J.M.)

Changes in host primary metabolism associated with the compatible interaction between cucumber mosaic virus and cotyledons of the marrow plant (*Cucurbita pepo* L.) have been localized, first by measuring activities of key enzymes in infected and uninfected regions of the cotyledon, and second by histochemical techniques applied to tissue prints of the infected region. A series of progressive metabolic changes occurs within the expanding infected lesion. Virus replication and the synthesis of viral protein at the periphery creates a strong sink demand associated with increased activities of anaplerotic enzymes, increased photosynthesis, and starch accumulation. Inside the lesion, when the synthesis of virus has declined, photosynthesis is reduced, starch is mobilized, and the emphasis of metabolism is shifted toward glycolysis and mitochondrial respiration. These changes are associated spatially with the onset of chlorosis. A decrease in total protein synthesis in this inner zone could be instrumental in some or all of these changes, leading to symptoms of viral infection.

Our recent studies of the interaction between CMV and the cotyledons of the marrow plant (*Cucurbita pepo* L.) have demonstrated the complexity of the metabolic responses to infection (Técsi et al., 1994a, 1994b). The first symptoms of CMV infection are circular chlorotic lesions 4 d after infection. We showed that such lesions are not homogeneous but constitute a dynamic structure composed of zones of cells of diverse physiology. Although particles accumulate throughout the lesion, circular zones of cells can be identified within the infected region. From the outside these are (a) a zone (i) of infected cells that do not accumulate starch, (b) a zone (ii) consisting of cells with increased photosynthetic activity, resulting in the accumulation of starch, (c) a zone (iii) of largely starchless cells that appear to have a low photosynthetic activity, and (d) a zone (iv) of cells surrounding the initial point of infection that retain high photosynthetic activity and a high starch content for the first 4 to 6 d postinfection. As the lesions expand during the course of infection, after 10 d the inner region (zones iii and

iv) becomes the dominant feature, leading to a generalized chlorosis. The fact that this inner zone is depleted of starch indicates that starch is being mobilized within cells at the inner border of the starch-containing zone (zone ii).

The infection process is accompanied in whole cotyledons by changes in many aspects of primary metabolism (Técsi et al., 1994a, 1994b). It is tempting to speculate that these changes occur specifically within zones of the lesion as direct or indirect responses to the progress of viral infection. For example, in intact cotyledons the rate of respiration and the capacities of the oxidative pentose phosphate pathway, glycolysis, and the Krebs cycle all increase in parallel with the expansion of the inner region of the lesion. Therefore, these increases could be associated with the respiration of the products of starch degradation in this inner region. An understanding of the development of lesions clearly requires information about the spatial distribution of changes in host metabolism in relation to virus replication in the infected cotyledon. To meet this requirement, we have developed novel methods to localize changes in a range of enzymes representative of key areas of metabolism. By dissecting lesions away from the surrounding uninfected tissue and by using histochemical techniques on tissue prints of discs of cotyledons in conjunction with video image analysis, we have correlated enzyme activities with the zones of the lesion identified previously (Técsi et al., 1994a). In addition, we have used in situ hybridization to locate viral nucleic acids and pulse-labeling with [^{35}S]Met to identify the sites of viral protein synthesis. These techniques allow us to propose a sequence of metabolic events following virus replication in a compatible host-virus interaction.

MATERIALS AND METHODS

Plant Material

Ten-day-old cotyledons of marrow plants (*Cucurbita pepo* L. cv Green Bush) were inoculated with the Kin strain of CMV as described previously (Técsi et al., 1994b).

Abbreviations: CMV, cucumber mosaic virus; NBT, nitroblue tetrazolium chloride; PMS, phenazine methosulfate.

Inoculation and Sampling

Inoculation was carried out according to Técsi et al. (1994b). Lesions were identified 3 d after inoculation as rings of high-fluorescence quenching of chlorophyll a following illumination (Técsi et al., 1994a). For enzyme activity measurements in extracts, cotyledons were sampled by excision of discs of 3 mm^2 from inside and outside the virus lesion, as well as from uninfected cotyledons. Samples were immediately frozen in liquid N_2 and stored at $-80°C$.

Measurement of Enzyme Activities in Extracts of Cotyledons

Extraction of enzymes and conditions for measurements of total activities of ADP-Glc pyrophosphorylase (EC 2.7.7.27), ATP-dependent phosphofructokinase (EC 2.7.1.11), Cyt c oxidase (EC 1.9.3.1), chloroplastic Fru bisphosphatase (EC 3.1.3.11), fumarate hydratase (EC 4.2.1.2), Glc-6-P dehydrogenase (EC 1.1.1.49), NAD-dependent isocitrate dehydrogenase (EC 1.1.1.42), NAD-dependent malate dehydrogenase (EC 1.1.1.37), NAD-dependent malic enzyme (EC 1.1.1.39), NADP-dependent malic enzyme (EC 1.1.1.40), PEP carboxylase (EC 4.1.1.31), 6-phosphogluconate dehydrogenase (EC 1.1.1.44), and total starch hydrolases were as described by Técsi et al. (1994b).

For additional enzyme assays, the reaction mixtures were as follows:

NADP-dependent glyceraldehyde-3-phosphate dehydrogenase (EC 1.2.1.13) (Kelly and Gibbs, 1973): 100 mM Bicine (pH 8.0), 0.2 mM NADPH, 10 mM $MgCl_2$, 4.5 mM ATP, 4 mM 3-phosphoglycerate, and 14 units mL^{-1} phosphoglycerate kinase.

NAD-dependent isocitrate dehydrogenase (EC 1.1.1.41) (Hathaway and Atkinson, 1963): 100 mM Hepes (pH 7.4), 4 mM $MnCl_2$, 2 mM NAD, and 5 mM DL-isocitrate.

NADP-dependent isocitrate dehydrogenase (EC 1.1.1.42) (Plaut and Sung, 1954): 100 mM Hepes (pH 7.4), 4 mM $MnCl_2$, 0.5 mM NADP, and 5 mM DL-isocitrate.

Ribulose-5-phosphate kinase (EC 5.3.1.16) (Leegood, 1990): 100 mM Bicine (pH 8.0), 10 mM MgCl2, 3 mM ATP, 50 mM KCl, 5 mM PEP, 0.5 mM ribulose-5-phosphate, 0.2 mM NADH, 8 units mL^{-1} pyruvate kinase, and 15 units mL^{-1} lactate dehydrogenase.

Peroxidase (EC 1.11.1.7) (Rathmell and Sequeira, 1974): 100 mM sodium citrate (pH 4.5), 0.5 mM guaiacol, and 12 μM H_2O_2.

Quantitation of Rubisco Protein and Chlorophyll

Rubisco protein content was determined by ELISA (Técsi et al., 1994b). Chlorophyll was measured as described by Leegood (1993).

Localization of Enzyme Activities on Tissue Prints

Tetrazolium and Diazo Salt Techniques (Gahan, 1984)

For localization of enzyme activity on tissue prints (Avidiushko et al., 1993), discs of cotyledon from which the lower epidermis had been removed were placed on posi-

tively charged nylon membrane (Boehringer Mannheim) dampened with enzyme extraction medium (Técsi, 1994b). Three pieces of filter paper were layered under the membrane and the whole sandwich was covered with a polyethylene sheet. The sandwich was pressed between metal plates (70 kg cm^{-2}, 5 s) and the pressed discs were removed and stained for starch (Técsi et al., 1994a). Tissue prints were briefly washed in 25 mM Hepes buffer (pH 7.4) and then incubated in a reaction mixture to develop insoluble, colored compounds at the sites of enzyme activity.

Enzymes and reaction mixtures were as follows:

ATP-dependent phosphofructokinase (EC 2.7.1.11): 200 mM Bicine (pH 8.0), 5 mM $MgCl_2$, 3 mM ATP, 2 mM NAD, 4 mM Fru-6-P, 5 mM Na_2HAsO_4, 1.2 units mL^{-1} aldolase, 2.4 units mL^{-1} glyceraldehyde-3-phosphate dehydrogenase, 0.8 mM NBT, and 0.4 mM PMS.

NADP-dependent glyceraldehyde-3-phosphate dehyrogenase (EC 1.2.1.13): 100 mM Bicine (pH 8.0), 0.5 mM NADP, 1 mM dihydroxyacetone phosphate, 5 mM Na_2HAsO_4, 20 units mL^{-1} triose-phosphate isomerase, 0.8 mM NBT, and 0.4 mM PMS.

Fumarate hydratase (EC 4.2.1.2), NADP-dependent malic enzyme (EC 1.1.1.40), and NAD-dependent isocitrate dehydrogenase (EC 1.1.1.42): the same as for enzyme activity measurements in extracts but with 0.8 mM NBT and 0.4 mM PMS.

NAD-dependent malic enzyme (EC 1.1.1.39): the same as for enzyme measurements in extracts but without DTT and with 0.8 mM NBT and 0.4 mM PMS.

Glc-6-P dehydrogenase (EC 1.1.1.49): 100 mM Hepes (pH 7.8), 0.5 mM NADP, 1.2 mM Glc-6-P, 5 mM $MgCl_2$, 4 mM maleimide, 0.8 mM NBT, and 0.4 mM PMS.

6-Phosphogluconate dehydrogenase (EC 1.1.1.44): 100 mM Hepes (pH 7.8), 0.5 mM NADP, 1.2 mM 6-phosphogluconate, 5 mM $MgCl_2$, 0.8 mM NBT, and 0.4 mM PMS.

Peroxidase (EC 1.11.1.7): 100 mM sodium citrate (pH 4.5), 2 mM p-phenylenediamine, and 4 mM catechol.

Cyt c oxidase (EC 1.9.3.1): 100 mM Hepes (pH 7.4), 20 μM Cyt c (reduced), and 3 mM 3,3-diaminobenzidine.

Starch Film Technique (Jacobsen and Knox, 1973; Steup, 1990)

For starch hydrolases (α-amylase, EC 3.2.1.1; β-amylase, EC 3.2.1.2; amyloglucosidase, EC 3.2.1.20; debranching enzyme, EC 3.2.1.10), dry nitrocellulose membrane (Whatman) was floated on the surface of an autoclaved, soluble starch solution (20 mg mL^{-1}) for 5 min at 25°C to create a starch film on its surface. The membrane was briefly washed in the reaction mixture containing 50 mM Mes and 2.5 mM $CaCl_2$, and tissue prints were made as described above. The tissue prints were then incubated in the same reaction mixture (37°C, 8 h). Finally, the undigested starch on the tissue prints was stained with 40 mM KI/I_2 solution.

In Situ Hybridization

In situ hybridization (Leitch et al., 1994) was performed on healthy and infected cotyledon tissue samples

collected 3 d postinfection. Lesions were localized by chlorophyll fluorescence imaging (Técsi et al., 1994a) and were excised with the surrounding uninfected tissue. The tissue samples were fixed and embedded (Leitch et al., 1994) with the modification of the fixative (20 mg mL^{-1} formaldehyde and 10 mg mL^{-1} Suc in 100 mM NaH$_2$PO$_4$, pH 7.2) and the embedding medium (Paraplast Xtra, Sigma). Consecutive 16-μm cross-sections through the lesions were cut on a microtome (Reichert, Vienna, Austria), and the sections were attached to microscope slides coated with 1 mg mL^{-1} poly-L-Lys (Sigma) and baked at 120°C for 2 h.

The cDNA template for the antisense RNA probe was prepared from a full-length, 2.2-kb cDNA clone in pUC9 vector (Boccard and Baulcombe, 1992) corresponding to the RNA3 of the virus. The cDNA template for the sense RNA probe was prepared by subcloning a 1.6-kb fragment of the full-length cDNA in the reverse direction into a pBS($-$) vector. After linearization with BglII restriction enzyme, digoxigenin-labeled antisense and sense RNA transcripts were prepared from these DNA templates with T7 RNA polymerase in the presence of digoxigenin-11-UTP (Boehringer Mannheim). The digoxigenin-labeled RNA transcripts were hydrolyzed in 100 mM NaHCO$_3$ (pH 10.2) to give fragments of approximately 0.3 kb in length. The sections were subjected to pronase digestion (0.68 units mL^{-1}, 25°C, 5 min) and postfixed in 40 mg mL^{-1} formaldehyde in maleic acid buffer saline (100 mM maleic acid, pH 7.5, 150 mM NaCl) (25°C, 10 min). After treatment with 0.5% (v/v) acetic anhydride in triethanolamine-HCl (pH 8.0), sections were rinsed in 200% (v/v) SSC buffer (15 mM sodium citrate, pH 7.0 , 150 mM NaCl) and dehydrated in ethanol series. Hybridizations of 200 ng mL^{-1} sense or antisense RNA probes were carried out in a hybridization mixture containing 50% (v/v) formamide, 10 mM DTT, 1 μg mL^{-1} RNA (type XXI from Sigma), 300 mM NaCl, 10 mM Tris-HCl (pH 6.8), 5 mM EDTA, 10 mM NaH$_2$PO$_4$, and 1 mg mL^{-1} blocking reagent for hybridization (Boehringer Mannheim). Slides were covered with coverslips of polypropylene foil and incubated in a humid chamber (50°C, 12 h). The coverslips were then carefully removed and the slides were washed in descending concentrations of SSC buffer (200% [v/v], 100% [v/v], 20% [v/v], and 10% [v/v]) containing 20 μg mL^{-1} SDS (50°C, 30 min for each step).

For immunological detection of the hybridized probe, the slides were incubated in blocking solution containing 1 mg mL^{-1} blocking reagent for hybridization (Boehringer Mannheim) in maleic acid buffer saline (37°C, 30 min). After incubation with 0.04% (v/v) anti-digoxigenin antibody-conjugate to alkaline phosphatase in the same blocking solution, color was developed in a reaction mixture containing 50 μg mL^{-1} 5-bromo-4-chloro-3-indolyl phosphate, 340 μg mL^{-1} NBT, 100 mM Tris-HCl (pH 9.50), 100 mM NaCl, and 5 mM MgCl$_2$.

The sections were counterstained with 1 mg mL^{-1} safranin microscopic stain (25°C, 2 min), dehydrated, and mounted in DePeX (Serva Feinbiochemica, Heidelberg, Germany).

Localization of Viral Coat Protein and Nucleic Acids on Tissue Prints

For localization of virus coat protein and nucleic acids, tissue prints were made in the same manner as described above but without dampening the nylon membrane, which was dried at 25°C after printing. The viral coat protein distribution on the tissue prints was detected by immunostaining (Técsi et al., 1994a). The viral nucleic acids on the tissue prints were hybridized with 200 ng mL^{-1} antisense or sense digoxigenin-labeled RNA probes and visualized according to the manufacturer's instructions (Boehringer Mannheim).

[^{35}S]Met Labeling of Cotyledon Discs

The lower epidermis of the cotyledon disc was removed and the discs were placed on the surface of a solution of 10 nM [^{35}S]Met (3.4 MBq mmol^{-1}) (Amersham) (25°C, 60 min, 150 μmol m^{-2} s^{-1} PPFD) in the wells of a plastic container. Immediately after labeling, the discs were fixed in 80% (v/v) ethanol at 95°C. Soluble compounds were removed by repeated extraction in 80% (v/v) ethanol and finally with water. Discs were placed on three layers of filter paper and covered with Benchkote (Whatman). The sandwich was pressed between metal blocks (70 kg cm^{-2}, 5 s) and the pressed discs were exposed to x-ray film (-20°C, 24 h).

Gel Electrophoresis, Immunoblotting, Autoradiography, and Quantitation of [^{35}S]Met Incorporation into Proteins

Discs of cotyledons were labeled with [^{35}S]Met as described above. The labeled discs were then rinsed briefly in H$_2$O, frozen in liquid N$_2$, and stored at -80°C. To separate proteins, discs at 3 d postinfection were homogenized in extraction medium containing 200 mM 2-amino-2-methylpropan-1-ol (pH 10.5), 5 mM DTT, and 35 mM SDS, and subjected to SDS-PAGE (15% acrylamide). To identify viral coat proteins, the separated proteins were transferred from the gel onto a PVDF membrane (Deutscher, 1990) that was immunostained with antibody to CMV particles according to Técsi et al. (1994a), omitting the healthy leaf sap from the blocking solution. The protein gel was dried and exposed to x-ray film (25°C, 21 d) to locate [^{35}S]Met incorporation. Bands were then excised from the gel and homogenized in water, and the radioactivity was counted in a scintillation counter.

Video Image Analysis of Tissue Prints and Printed Tissue

Both the tissue print stained with various techniques and the corresponding starch-stained leaf tissue were photographed with a photomicroscope (Reichert). The enlarged photographs of the lesions were subjected to quantitative video image analysis by scanning across the diameters of the randomly chosen, corresponding lesions on 5 to 10 cotyledon discs. Quantification of the optical density on the captured image was carried out on 150 measurement points extending 2 mm in a straight line on either side of the center of the lesion. At each measurement point the gray values were extracted using OPTIMAS 4.02 (BioScan,

Washington, DC) image-analyzing software. This data set from an individual lesion represented one replicate. The replicate data sets (between 9 and 27) were then averaged and plotted against the distance across the lesion using the Excel 4.0 (Microsoft, Redmond, WA) and SigmaPlot 2.01 (Jandel Scientific, Erkrath, Germany) software packages.

RESULTS

Enzyme Localization within Infected Cotyledons

We first determined whether the activities of a range of enzymes involved in carbon metabolism were altered in the lesions at an early stage of development, 3 d postinfection, before the onset of symptoms. Lesions were identified as zones of high fluorescence quenching of chlorophyll a following illumination (Técsi et al., 1994a). Apparently healthy tissue taken from outside the lesions in infected cotyledons and tissue from within the lesions themselves were compared with tissue from uninfected cotyledons in assays to determine a range of enzymes and chlorophyll. The chlorophyll content in the lesions was not significantly reduced at this stage of infection (Table I). A mild chlorosis started to occur in the middle of the lesion only from approximately d 4 postinfection. Table I shows that en-

zyme activities in healthy regions of infected and uninfected cotyledons were not significantly different; however, the lesions showed alterations in the activities of all of the enzymes measured.

Elevation in the activities of a number of enzymes were seen in the lesions when they were compared with healthy tissue. These included enzymes associated with glycolysis (ATP-dependent phosphofructokinase), the entry of carbon into the Krebs cycle (NAD-dependent malic enzyme, PEP carboxylase), the Krebs cycle (NAD-dependent isocitrate dehydrogenase, fumarate hydratase), the mitochondrial electron transport chain (Cyt c oxidase), key enzymes of the oxidative pentose phosphate pathway (Glc-6-P dehydrogenase and 6-phosphogluconate dehydrogenase), and other anaplerotic reactions (NADP-dependent malic enzyme, NADP-dependent isocitrate dehydrogenase). Other enzymes that increased in activity included those involved in starch degradation (starch hydrolases) and peroxidase, which increased in activity nearly 5-fold in the lesion compared with healthy tissue.

The activities or amounts of some enzymes declined in the lesions compared with healthy tissue. These included three enzymes of the Benson-Calvin cycle (Rubisco, NADP-dependent glyceraldehyde-3-phosphate dehydrogenase,

Table I. *Total activity/total amount of key enzymes of the main metabolic pathways and chlorophyll content in uninfected as well as outside and inside the lesions in virus-infected C. pepo cotyledon on d 3 postinfection*

Cotyledons were sampled by excision of small discs of 3 mm² from outside and inside of the virus lesion. Enzyme activities were detected as described in "Materials and Methods." Rubisco content was determined by the ELISA technique. Chlorophyll content was measured spectrophotometrically in cotyledon extracts prepared in 80% (v/v) acetone. Data are expressed on a leaf area basis (enzyme activities in μmol m^{-2} s^{-1}, chlorophyll and Rubisco contents in g m^{-2}). Values are means of replicates of between 8 and 16 separate experiments. Ranges indicate confidence intervals at the 90% level.

Enzyme/Metabolite	Healthy	Infected	
		Outside lesion	Within lesion
		μmol m^{-2} s^{-1}	
Glycolysis and mitochondrial respiration			
ATP-dependent phosphofructokinase	0.47 ± 0.06	0.65 ± 0.13	1.05 ± 0.10
NAD-dependent malic enzyme	3.60 ± 0.52	3.58 ± 0.56	6.23 ± 0.64
PEP carboxylase	8.19 ± 1.19	7.28 ± 1.42	13.17 ± 1.45
NAD-dependent isocitrate dehydrogenase	0.64 ± 0.11	0.65 ± 0.11	1.31 ± 0.20
Fumarate hydratase	9.6 ± 1.3	8.8 ± 1.1	21.3 ± 1.8
Cyt c oxidase	6.5 ± 1.6	7.3 ± 1.1	11.0 ± 2.6
Anaplerotic reactions			
Glc-6-P dehydrogenase	2.39 ± 0.47	2.44 ± 0.63	9.68 ± 1.36
6-Phosphogluconate dehydrogenase	2.96 ± 0.57	3.05 ± 0.32	7.32 ± 0.62
NADP-dependent malic enzyme	6.8 ± 0.6	7.4 ± 0.9	12.6 ± 1.0
NADP-dependent isocitrate dehydrogenase	7.8 ± 1.1	8.0 ± 1.1	12.9 ± 0.9
Starch metabolism			
Total starch hydrolase	0.110 ± 0.022	0.105 ± 0.025	0.289 ± 0.028
ADP-Glc pyrophosphorylase	2.71 ± 0.08	2.70 ± 0.25	1.96 ± 0.07
Photosynthesis			
Chlorophyll[a]	0.672 ± 0.036	0.637 ± 0.037	0.594 ± 0.037
Rubisco[a]	2.59 ± 0.30	2.58 ± 0.22	2.03 ± 0.16
NADP-dependent glyceraldehyde-3-phosphate dehydrogenase	22.2 ± 1.9	21.6 ± 2.3	15.8 ± 2.0
Ribulose-5-phosphate kinase	167 ± 30	169 ± 26	123 ± 20
Chloroplastic Fru-1,6-bisphosphatase	3.89 ± 0.58	4.07 ± 0.80	5.06 ± 0.65
Peroxidase	14.0 ± 3.0	18.4 ± 5.7	103.2 ± 26.7

[a] g m^{-2}.

and ribulose-5-phosphate kinase) and a key enzyme involved in starch synthesis (ADP-Glc pyrophosphorylase). Unlike the other enzymes of the Benson-Calvin cycle, the activity of the chloroplastic Fru-1,6-bisphosphatase did not change significantly.

Enzyme Localization within Lesions

The dissection of lesions gave information about the quantitative changes in enzyme activity between lesions and healthy tissue, but not about the spatial distribution of the activity of an enzyme within the lesion. To obtain this information, we blotted discs excised from cotyledons onto a nylon membrane and assayed the enzyme activity in situ on the tissue print. The distribution of the activity was then related to the distribution of starch in the lesion following iodine staining of the pressed tissue disc. Figure 1 shows a typical example of the in situ enzyme assay (top right) and its corresponding tissue disc stained for starch (bottom right) for each enzyme. Enlarged photographs of the activity and starch stains were subjected to video image analysis. The data obtained from the corresponding lesions stained for activity and starch were averaged to provide a qualitative picture of changes in enzyme activity across the lesion (Fig. 1, graphs). To confirm that the images reflected enzyme activity, control tissue prints were incubated under conditions identical to those used for enzyme detection but without a key substrate of the enzyme; lesions were not visible under these conditions for any of the enzymes (data not shown).

Image analysis of the iodine-stained discs, from which prints were taken for each enzyme, clearly revealed the outer starch ring (zone ii) and sometimes the central dot of starch (zone iv). These were employed as reference points for the structure of the lesion and its various zones (Técsi et al., 1995). The scans of enzyme activity showed four distinct and reproducible patterns, suggesting that the patterns observed do not arise by differential permeability of certain areas of the lesion during blotting and that they accurately reflect the distribution of enzyme activities between different zones of the lesion:

(i) Enzymes associated with glycolysis (ATP-dependent phosphofructokinase, Fig. 1A) and respiration (NAD-dependent malic enzyme, Fig. 1B; NAD-dependent isocitrate dehydrogenase, Fig. 1C; fumarate hydratase, Fig. 1D; Cyt *c* oxidase, Fig. 1E) showed increased activity restricted to the inner region of the lesion, rising to a peak of activity at the center of the lesion. Total starch hydrolase activity (Fig. 1F) also rose in this inner region. Unfortunately, the activity of ADP-Glc pyrophosphorylase, an enzyme associated with starch biosynthesis, could not be detected reliably on tissue prints.

(ii) Activities of enzymes involved in the oxidative pentose-phosphate pathway (Glc-6-P dehydrogenase, Fig. 1G; 6-phosphogluconate dehydrogenase, Fig. 1H) and of peroxidase (Fig. 1I) were elevated more or less uniformly across the lesion, although there was evidence in each case of a slightly elevated activity associated with the outer starch ring.

(iii) The activity of NADP-dependent malic enzyme (Fig. 1J) was clearly elevated outside the starch ring but was lower both in adjacent healthy tissue and in the central zone of the lesion.

(iv) The activity of NADP-dependent glyceraldehyde-3-phosphate dehydrogenase (Fig. 1K) steadily declined from the periphery to the center of the lesion. It was not possible to measure the activities of other Benson-Calvin cycle enzymes on tissue prints.

Location of Viral Multiplication

Two methods were used to investigate the site of viral replication. CMV has a positive-strand RNA, and replication involves the synthesis of a complementary negative strand. In situ hybridization was used to determine the distribution of the positive and negative strands of the viral RNA in both tissue prints and sections of cotyledons.

Consecutive sections of an infected lesion stained for either viral coat protein by immunocytochemistry or for positive or negative senses of the viral genome by in situ hybridization (Fig. 2) showed that there was a very sharp transition between uninfected and infected regions of the leaf, implying that maximal virus replication occurred at the edge of the advancing lesion. However, the correspondence in the location of these target molecules did not allow us to determine the site of virus replication definitively. A similar distribution of viral protein (Fig. 3A) and RNAs (Fig. 3, B and C) was observed when the two techniques were carried out on tissue prints, although analysis of the scanned images did appear to show accumulation of the negative sense viral RNA (Fig. 3C) replication immediately outside of the major zone of positive sense viral RNA accumulation.

As an alternative method of investigating the region of viral replication, we supplied the cotyledons with [^{35}S]Met in the light to determine if there was a region in which the rate of protein synthesis was elevated. Leaf discs were then extracted in ethanol to remove soluble radioactivity and autoradiographed. These autoradiographs revealed a clear ring structure associated with an increased incorporation of [^{35}S]Met (Fig. 4). The region of maximum incorporation was outside the starch ring; incorporation declined within the starch ring to a level lower than in the regions of apparently healthy tissue outside the lesions. We then determined which polypeptides were labeled by subjecting extracts of [^{35}S]Met-labeled discs of cotyledons to SDS-PAGE, immunoblotting, and autoradiography (Fig. 5). Staining of the separated polypeptides (Fig. 5) revealed the presence of an infection-specific band at 30 kD (Fig. 5, arrowheads). Immunoblot analysis with anti-viral coat protein serum (Fig. 5) showed the major band to be the viral coat protein (the actual molecular mass of this protein subunit is 25 kD; Palukaitis et al., 1992). The nature of the minor viral band at 52 kD is not known. The autoradiograph of labeled proteins (Fig. 5) revealed a number of labeled bands, including the viral coat protein at 30 kD. This was confirmed by immunoprecipitation. Excision of the 30-kD band revealed that it contained approximately
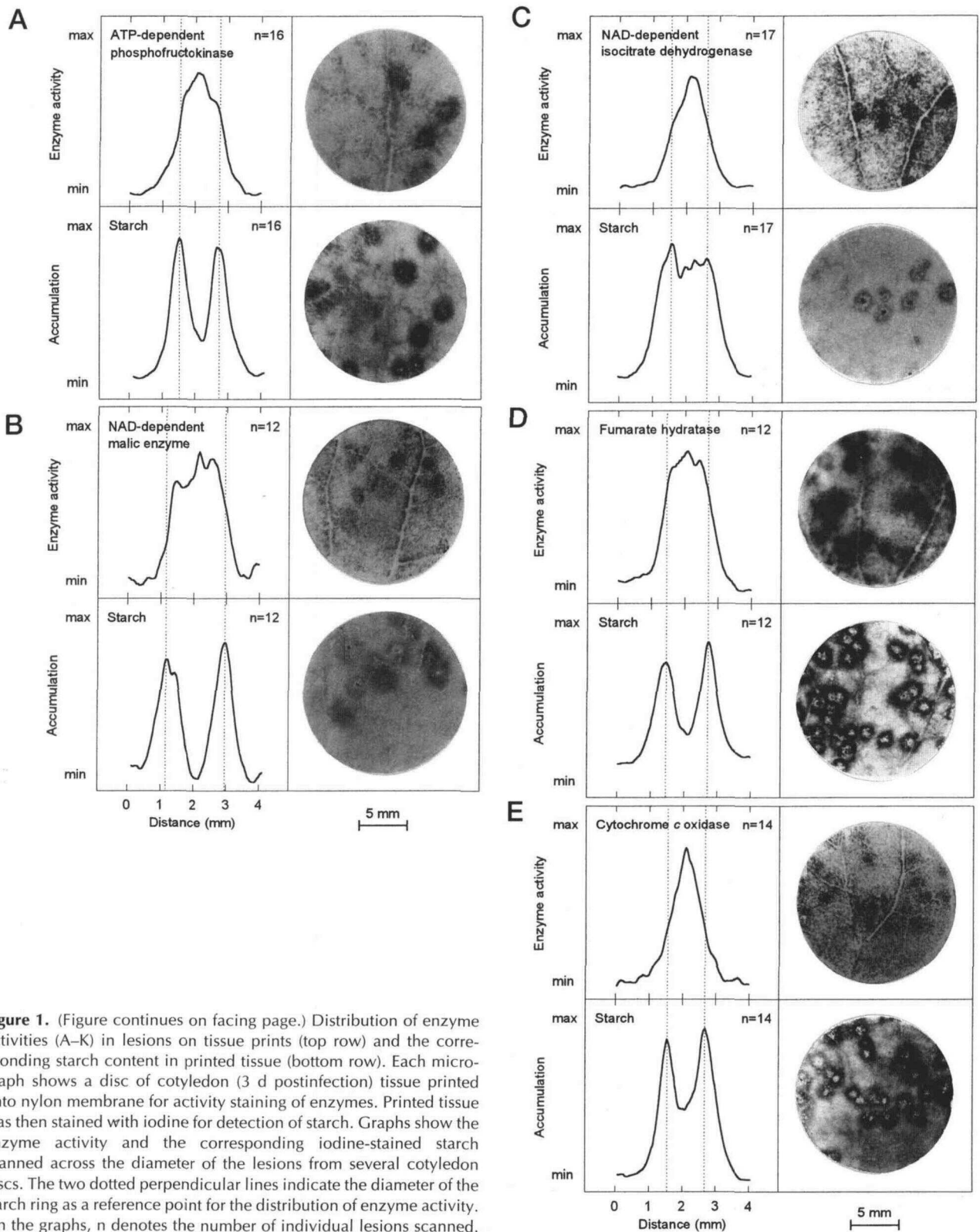
Figure 1. (Figure continues on facing page.) Distribution of enzyme activities (A–K) in lesions on tissue prints (top row) and the corresponding starch content in printed tissue (bottom row). Each micrograph shows a disc of cotyledon (3 d postinfection) tissue printed onto nylon membrane for activity staining of enzymes. Printed tissue was then stained with iodine for detection of starch. Graphs show the enzyme activity and the corresponding iodine-stained starch scanned across the diameter of the lesions from several cotyledon discs. The two dotted perpendicular lines indicate the diameter of the starch ring as a reference point for the distribution of enzyme activity. On the graphs, n denotes the number of individual lesions scanned.
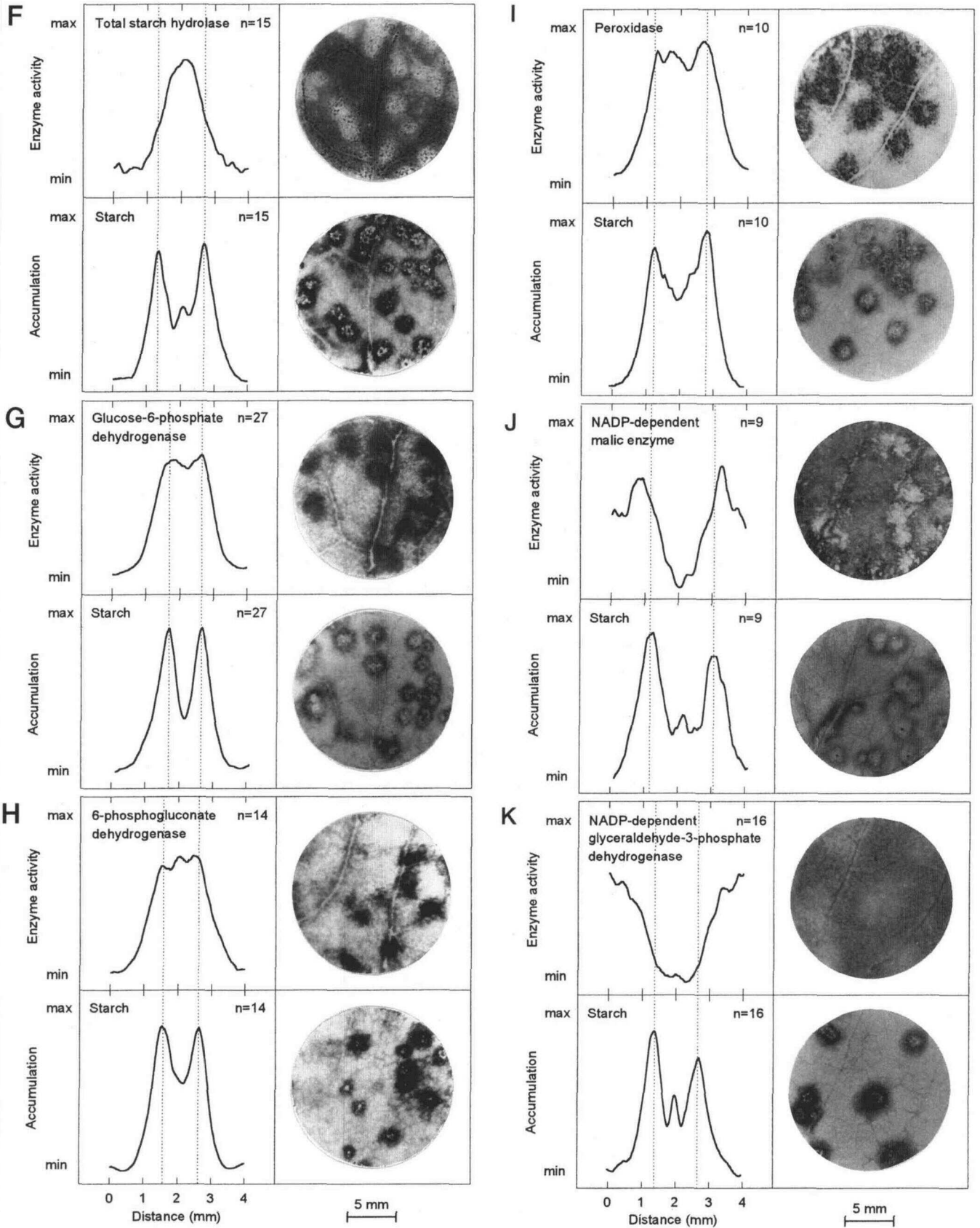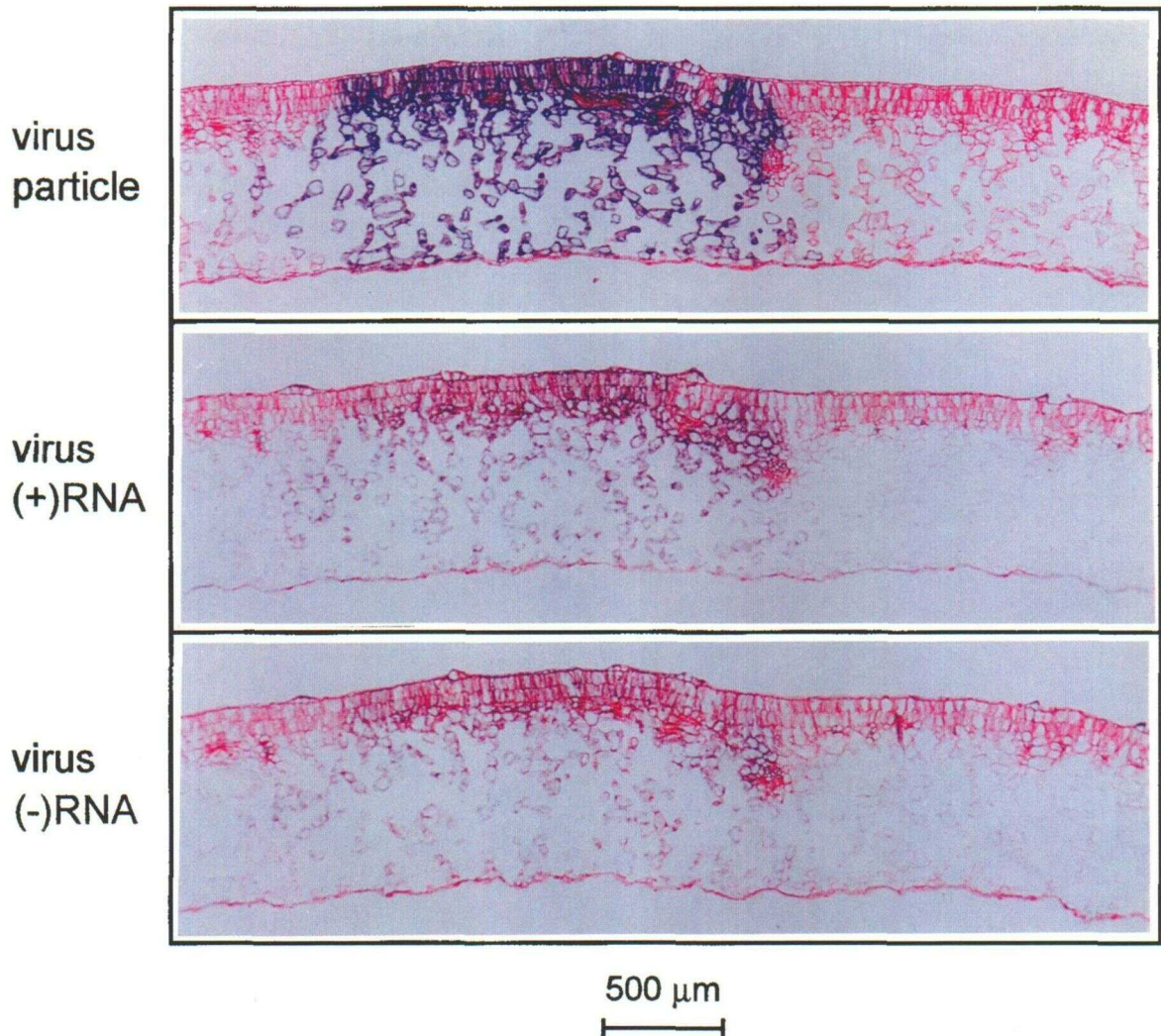
Figure 1. (Continued from facing page.)

Figure 2. Distribution of virus particles, (+)RNA, and (−)RNA of the virus in radial cross-sections of a single lesion in an infected cotyledon. The micrographs show consecutive cross-sections through the center of a single lesion on d 4 postinfection. The sections were subjected to immunostaining for virus particles (blue stain) as well as nonradioactive in situ hybridization to (+)RNA and (−)RNA of the virus (blue stain), followed by counterstaining with safranin (red stain). The region occupied by the lesion is indicated by the presence of the virus particles (Técsi et al., 1994a).

10% of the total radioactivity incorporated into polypeptides on the gel. Since incorporation of [35S]Met into coat protein is likely to occur only in a discrete zone (Fig. 4) within the lesion, coat protein must represent a very high proportion of the protein synthesized in this zone.

DISCUSSION

The work reported in this and our earlier papers shows that the infection of marrow cotyledons by CMV has a large stimulatory effect on the rate of respiration, the capacities of the oxidative pentose phosphate pathway, glycolysis, the Krebs cycle, anaplerotic reactions, mitochondrial electron transport, and starch degradation. The capacities for starch synthesis and the Benson-Calvin cycle decline. These effects are essentially confined to the lesions; tissue from outside the lesions on infected cotyledons is not

distinguishable in any of these respects from healthy tissue. Although these observations are an advance on biochemical analyses of whole, infected tissues (Técsi et al., 1994b), they do not provide information about changes occurring within individual lesions during their development. Our earlier work showed that zones of cells within the lesion differ markedly from one another in their rates of photosynthesis and starch metabolism, suggesting that virus infection causes profound and progressive perturbation of primary metabolism in infected cells. The novel method of scanning histochemical prints of lesions using video image analysis has enabled us to confirm and greatly extend these observations and to attribute changes in enzyme activities measured on a whole-cotyledon or whole-lesion basis to specific zones of cells within the lesion.

Two different techniques showed (Figs. 2 and 3) that virus particles and the positive and negative sense viral
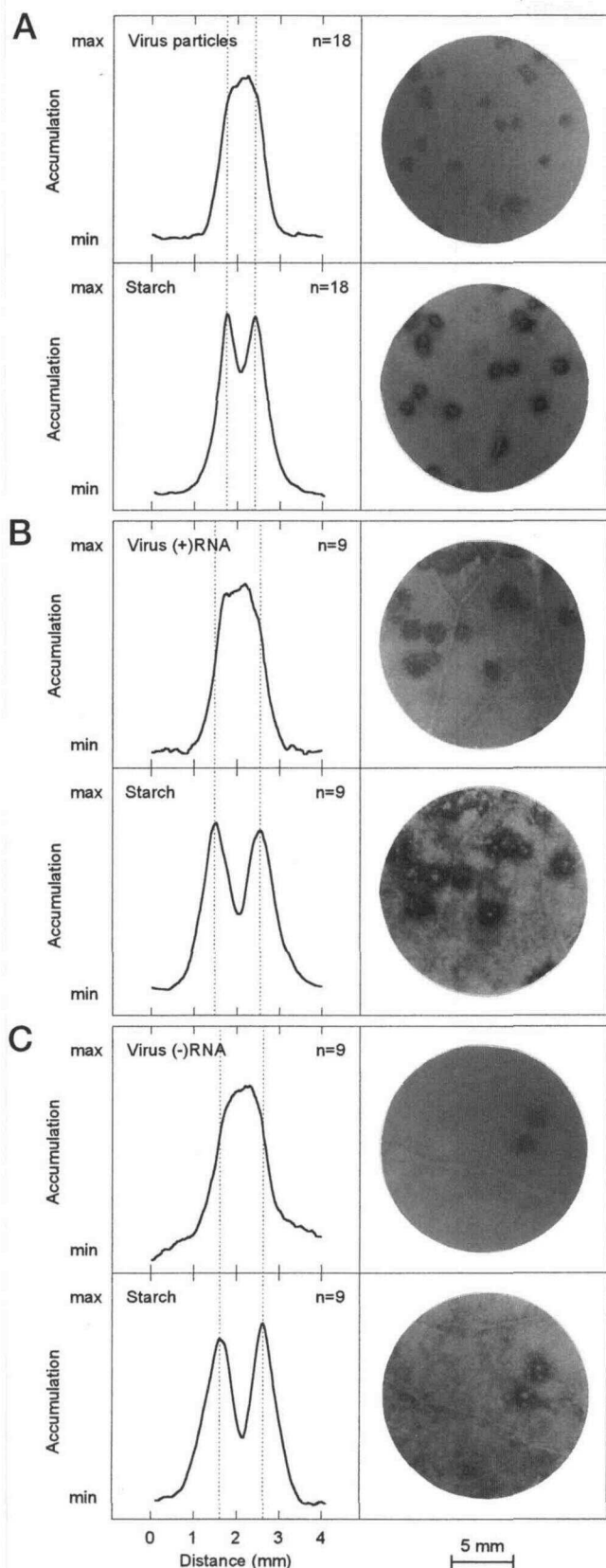
RNA were all present throughout the lesion, and therefore did not unequivocally identify the site of virus replication. This result is different from that obtained for another RNA virus replicating in pea tissue (Wang and Maule, 1995), where the location of the negative sense viral RNA only in cells close to the advancing infection front indicated a tightly restricted zone of virus multiplication. We must conclude that in this host-virus system viral negative sense RNA has greater stability than in the pea system. However, two pieces of information for CMV in marrow cotyledons suggest that virus replication is also concentrated at the infection front. First was evidence of accumulation of negative sense viral RNA in advance of the major increase in accumulation of positive sense viral RNA (Fig. 3), and second was the clear incorporation of [^{35}S]Met into viral coat protein at the infection front (Fig. 4). The extent of coat protein synthesis (10% of total protein synthesis in excised lesions containing all of the infected tissue and peripheral uninfected tissue) suggests that at the lesion edge there must be a major diversion of protein-synthesizing capacity toward viral products. We might expect, therefore, that the requirements for the synthesis of viral RNA and proteins would result in metabolic changes at the infection front that need not necessarily be sustained deeper in the infected area, but which may have longer-term metabolic repercussions. Hence, we might see zonal changes that lead eventually to symptom expression. Our results are consistent with these expectations. By treating the expanding lesion as a dynamic structure, a series of programmed biochemical responses to infection can be inferred (Fig. 6).

Associated with a need for increased biosynthetic capacity, the earliest metabolic response we recorded was a transient increase in NADP-dependent malic enzyme, an activity probably important in anaplerotic pathways. This was supported by a more sustained increase in the activities of enzymes of the oxidative pentose phosphate pathway (Glc-6-P dehydrogenase, 6-phosphogluconate dehydrogenase). We have shown previously (Técsi et al., 1994a) that following virus invasion there is an increase in photosynthetic capacity in the outer zone of the lesion and an associated accumulation of starch in cells immediately behind the infection front. Whether this increase in photosynthetic capacity is directly stimulated by a product of virus multiplication is unclear at this time, but it could provide the necessary source of assimilated carbon to support a burst of synthesis of virus-specific products. The photosynthetic enzymes NADP-

Figure 3. Distribution of virus particles (A), (+)RNA (B), and (−)RNA (C) of the virus in the lesion on tissue prints (top row) and the corresponding starch content in printed tissue (bottom row). Each micrograph shows a disc of cotyledon (3 d postinfection) tissue printed onto nylon membrane for immunostaining virus particles and hybridization staining of nucleic acids. Printed tissue was stained with iodine for detection of starch. Graphs show the immunostained, hybridization-stained tissue prints and the iodine-stained printed tissues scanned across the diameter of the lesion. The two dotted perpendicular lines indicate the diameter of the starch ring as a reference point for the distribution of enzyme activity. On the graphs, n denotes the number of individual lesions scanned.
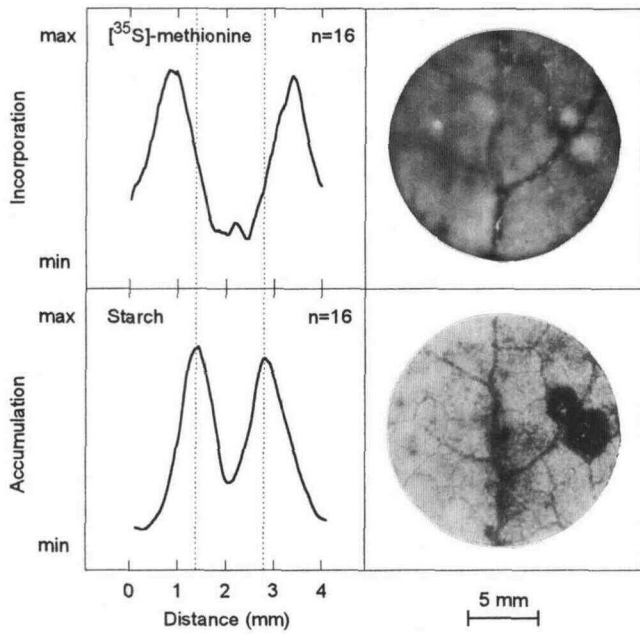
Figure 4. Distribution of [^{35}S]Met incorporation in the lesions on autoradiographs (top row) and the corresponding starch accumulation in cotyledon disc (bottom row). Each micrograph shows a disc of cotyledon (3 d postinfection) incubated in [^{35}S]Met solution for 60 min. After removing soluble compounds it was exposed to x-ray film (top row) and then stained with iodine for detection of starch. Graphs show the autoradiographs of [^{35}S]Met incorporation and iodine-stained starch scanned across the diameter of the lesions. The two dotted perpendicular lines indicate the diameter of the starch ring as a reference point to the distribution of [^{35}S]Met incorporation in the lesion. On the graphs, n denotes the number of separate lesions scanned.
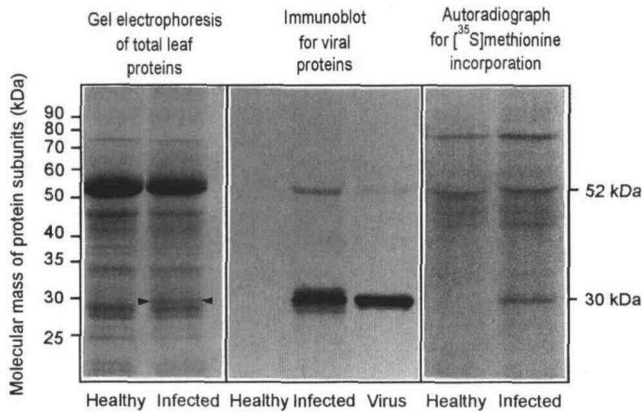
Figure 5. Gel electrophoresis, immunoblotting, and autoradiography of proteins labeled with [^{35}S]Met. To separate proteins, extracts of [^{35}S]Met-labeled cotyledon discs harvested 3 d postinfection were subjected to SDS-PAGE. To identify viral coat proteins, the blot from the electrophoretogram of healthy, infected, and purified virus particles was immunostained. To detect [^{35}S]Met incorporation, the electrophoretogram was autoradiographed. Arrowheads show the presence of a viral coat protein band at 30 kD in infected tissue. The autoradiograph revealed a heavily labeled band at this molecular mass. The immunoblot confirms that this band may be attributed to the virus particles.
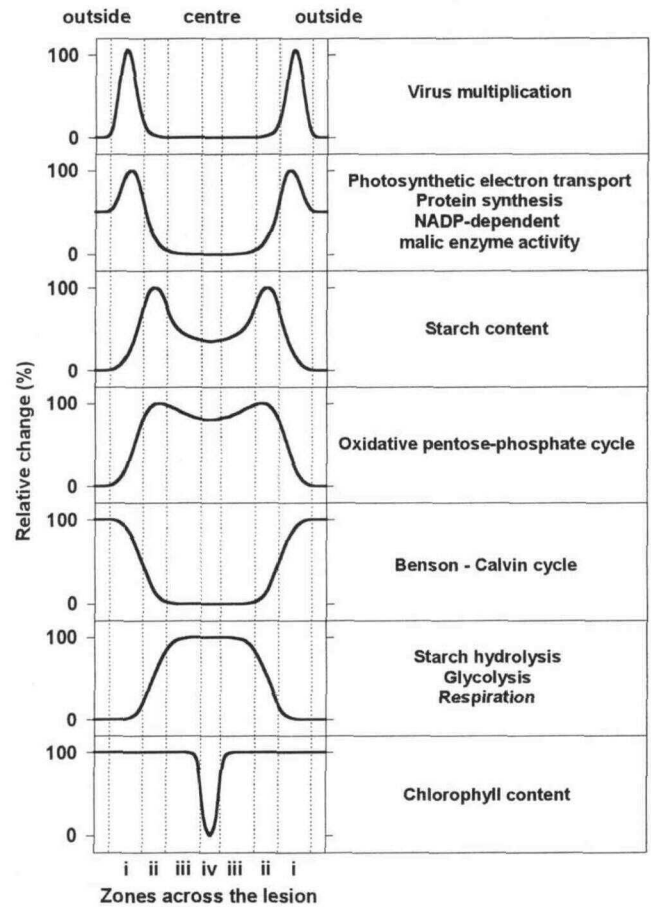
Figure 6. Relative changes in a series of biochemical responses to infection across the virus lesion. The extreme values of the graphs in the left-hand column represent the minimal (0%) and the maximal (100%) observed values of each parameter shown on the right. The circular zones of cells (i–iv) across the lesion are indicated with perpendicular dotted lines. At the sites of virus replication, protein synthesis and the activity of NADP-dependent malic enzyme are stimulated. The rate of the photosynthetic electron transport is also *stimulated at this region during the induction phase of photosynthesis* but is lower in the center of the lesion even during steady-state photosynthesis (L.I. Técsi, unpublished results). Inside the lesion, *starch accumulates and other biosynthetic processes are elevated,* as indicated by the increased activity of the enzymes of the oxidative pentose-phosphate cycle. At the same time, the activities of enzymes of the *Benson-Calvin cycle decline. Finally, starch degradation, gly-*colysis, and respiration are activated and chlorosis (visual observation) starts developing in the center of the lesion.

dependent glyceraldehyde-3-phosphate dehydrogenase (Fig. 1K), Rubisco, ribulose-5-phosphate kinase, and Fru-1,6-bisphosphatase (Table I) do not increase in parallel with the increase in photosynthesis, suggesting that, unlike respiration and glycolysis in the center of the lesion, this increase can be achieved without stimulating enzyme activity.

Inside the zone of starch accumulation a wide range of changes can be seen. Increases in starch hydrolase activity correlate with the loss of starch, but there are also changes that carry broader implications. There is a decrease in total

protein synthesis after the phase of virus replication has passed, and there are decreases in the activities of photosynthetic enzymes inside the zone of starch accumulation. The enzyme activities associated with glycolysis and respiration all increase in the central region of the lesion, although their precise distributions in this area may differ slightly. Peroxidase (Fig. 1I), an enzyme widely implicated in host responses to pathogen attack (e.g. Ye et al., 1990), showed increased activity through the area of starch accumulation to the center of the lesion. The biological role of this enzyme in compatible interactions such as CMV in marrow has yet to be determined.

The complexity of mosaic lesions suggests that viral infection could interfere with the normal carbohydrate metabolism of leaf cells in more than one way. The pattern of altered physiology is indicative of a series of metabolic events occurring over several days following viral replication within a cell. The present results provide evidence that in marrow cotyledons the virus does not act as a general sink for carbon and nitrogen at the level of the whole cotyledon (see also Técsi et al., 1994b), although in cells in which virus is actively replicating it may constitute a very powerful sink. Hence, the elevation of biosynthetic capacity, reflected in the increased activities of enzymes of the oxidative pentose phosphate pathway and of NADP-dependent malic enzyme at the periphery of the lesion, may occur in response to sink demand created by viral replication.

We do not yet know how these metabolic changes are induced. It may be that the virus has an immediate effect on the expression of host genes. Recent work on pea embryos infected with seed-borne mosaic virus has shown that virus replication is restricted to a zone of cells close to the infection front. In situ hybridization probes for nine genes from two pathways of metabolism failed to detect RNA transcripts within this zone, although transcripts were found in similar amounts in tissues on either side of the zone (Wang and Maule, 1995). Alternatively, there may be less direct causes, e.g. the disruption of cell-to-cell communication or other action attributable to the activity of viral movement proteins. Studies of transgenic tobacco expressing the tobacco mosaic virus movement protein show alterations in carbon partitioning that are unrelated to modifications of the plasmodesmatal size-exclusion limit. It has been suggested that the movement protein interferes with an endogenous signal transduction pathway that involves macromolecular trafficking through plasmodesmata to regulate biomass partitioning (Balachandran et al., 1995; Olesinski et al., 1995). Any or all of these processes may apply in the case of CMV infections of the marrow plant. The end result of all of these changes is the appearance of disease symptoms, in this case, chlorosis on the inoculated and systemically infected leaves. We have shown that chlorosis is correlated spatially with increased glycolysis and respiration, decreased photosynthesis, and a reduction in total protein synthesis. Identification of the primary causative agent of chlorotic symptoms awaits further analysis.

ACKNOWLEDGMENT

LITERATURE CITED

Avidiushko SA, Ye XS, Kuc J (1993) Detection of several enzymatic activities in leaf prints of cucumber plant. Physiol Mol Plant Pathol 42: 441–454

Balachandran S, Hull RJ, Vaadia Y, Wolf S, Lucas WJ (1995) Alteration in carbon partitioning induced by the movement protein of tobacco mosaic virus originates in the mesophyll and is independent of change in the plasmodesmatal size exclusion limit. Plant Cell Environ 18: 1301–1310

Boccard F, Baulcombe DC (1992) Infectious in vitro transcripts from amplified cDNAs of the Y and Kin strains of cucumber mosaic virus. Gene 114: 223–227

Deutscher MP (1990) Guide to Protein Purification. Academic Press, London

Gahan PB (1984) Plant Histochemistry and Cytochemistry. Academic Press, London

Hathaway JA, Atkinson DE (1963) The effect of adenylic acid on yeast nicotinamide adenine dinucleotide isocitrate dehydrogenase, a possible metabolic control mechanism. J Biol Chem 238: 2875–2881

Jacobsen JV, Knox RB (1973) Cytochemical localization and antigenicity of α-amylase in barley aleurone tissue. Planta 112: 213–224

Kelly GJ, Gibbs M (1973) Non-reversible D-glyceraldehyde 3-phosphate dehydrogenase of plant tissues. Plant Physiol 52: 111–118

Leegood RC (1990) Enzymes of the Calvin cycle. In PM Dey, JB Harborne, eds, Enzymes in Plant Biochemistry: Enzymes of Primary Metabolism, Vol 3. Academic Press, London, pp 15–37

Leegood RC (1993) Carbon metabolism. In DO Hall, JMO Scurlock, HR Bolhàr-Nordenkampf, RC Leegood, SP Long, eds, Photosynthesis and Production in a Changing Environment: A Field and Laboratory Manual. Chapman and Hall, London, pp 247–267

Leitch AR, Schwarzacher T, Jackson D, Leitch IR (1994) In Situ Hybridization: A Practical Guide. Bios Scientific Publishers, Oxford, UK

Olesinski AA, Lucas WJ, Galun E, Wolf S (1995) Pleiotropic effects of tobacco-mosaic-virus movement protein on carbon metabolism in transgenic tobacco plants. Planta 197: 118–126

Palukaitis P, Roossinck MJ, Dietzgen RG, Francki RIB (1992) Cucumber mosaic virus. Adv Virus Res 41: 281–348

Plaut GWE, Sung S-C (1954) Diphosphopyridine nucleotide isocitric dehydrogenase from animal tissues. J Biol Chem 207: 305–314

Rathmell WG, Sequeira L (1974) Soluble peroxidase in fluid from the intercellular spaces of tobacco leaves. Plant Physiol 53: 317–318

Steup M (1990) Starch degrading enzymes. In PJ Lea, ed, Methods in Plant Biochemistry, Vol 2. Academic Press, New York, pp 103–128

Técsi LI, Maule AJ, Smith AM, Leegood RC (1994a) Complex, localised changes in CO_2 assimilation and starch content associated with the susceptible interaction between cucumber mosaic virus and a cucurbit host. Plant J 5: 837–847

Técsi LI, Maule AJ, Smith AM, Leegood RC (1994b) Metabolic alterations in cotyledons of Cucurbita pepo infected by cucumber mosaic virus. J Exp Bot 45: 1541–1551

Técsi LI, Smith AM, Maule AJ, Leegood RC (1995) Physiological studies of viral mosaic infection. In DR Walters, JD Scholes, RJ Bryson, ND Paul, N McRoberts, eds, Physiological Responses of Plants to Pathogens: Aspects of Applied Biology, Vol 42. Association of Applied Biologists, Wellesbourne, UK, pp 133–140

Wang D, Maule AJ (1995) Inhibition of host gene expression associated with plant virus replication. Science 267: 229–231

Ye XS, Pan SQ, Kuc J (1990) Activity, isozyme pattern, and cellular localization of peroxidase as related to systemic resistance of tobacco to blue mold (Peronospora tabacina) and tobacco mosaic virus. Phytopathology 80: 1295–1299